

# Soft Matter

Accepted Manuscript



This is an *Accepted Manuscript*, which has been through the Royal Society of Chemistry peer review process and has been accepted for publication.

*Accepted Manuscripts* are published online shortly after acceptance, before technical editing, formatting and proof reading. Using this free service, authors can make their results available to the community, in citable form, before we publish the edited article. We will replace this *Accepted Manuscript* with the edited and formatted *Advance Article* as soon as it is available.

You can find more information about *Accepted Manuscripts* in the [Information for Authors](#).

Please note that technical editing may introduce minor changes to the text and/or graphics, which may alter content. The journal's standard [Terms & Conditions](#) and the [Ethical guidelines](#) still apply. In no event shall the Royal Society of Chemistry be held responsible for any errors or omissions in this *Accepted Manuscript* or any consequences arising from the use of any information it contains.

## ARTICLE

# Prediction and Validation of Diffusion Coefficients in a Model Drug Delivery System Using Microsecond Atomistic Molecular Dynamics Simulation and Vapour Sorption Analysis

Cite this: DOI: 10.1039/x0xx00000x

Received 13th June 2014,  
Accepted 13th June 2014

DOI: 10.1039/x0xx00000x

www.rsc.org/

Christopher Forrey,<sup>a</sup> David M. Saylor,<sup>a</sup> Joshua S. Silverstein,<sup>a</sup> Jack F. Douglas,<sup>b</sup> Eric M. Davis,<sup>b</sup> and Yossef A. Elabd.<sup>c</sup>

Diffusion of small to medium sized molecules in polymeric medical device materials underlies a broad range of public health concerns related to unintended leaching from or uptake into implantable medical devices. However, obtaining accurate diffusion coefficients for such systems at physiological temperature represents a formidable challenge, both experimentally and computationally. While molecular dynamics simulation has been used to accurately predict the diffusion coefficients,  $D$ , of a handful of gases in various polymers, this success has not been extended to molecules larger than gases, e.g., condensable vapors, liquids, drugs. We present atomistic molecular dynamics simulation predictions of diffusion in a model drug eluting system that represent a dramatic improvement in accuracy compared to previous simulation predictions for comparable systems. We find that, for simulations of insufficient duration, sub-diffusive dynamics can lead to dramatic over-prediction of  $D$ . We present useful metrics for monitoring the extent of sub-diffusive dynamics and explore how these metrics correlate to error in  $D$ . We also identify a relationship between diffusion and fast dynamics in our system, which may serve as a means to more rapidly predict diffusion in slowly diffusing systems. Our work provides important precedent and essential insights for utilizing atomistic molecular dynamics simulations to predict diffusion coefficients of small to medium sized molecules in condensed soft matter systems.

## Introduction

Composite drug-polymer systems have long played a pivotal role in controlled release and targeted drug delivery applications.<sup>1</sup> While a great diversity of potential delivery strategies exist due to the nearly limitless variety of synthetic polymers available and to the numerous options for drug-polymer association, most approaches essentially involve encasing drug in some way within polymer. The polymer then acts as an engineered diffusive barrier,<sup>2-4</sup> selectively regulating chemical transport to achieve the desired drug release profile while simultaneously impeding the ingress of physiological fluids. Diffusion is thus ultimately the means through which the polymer mediates molecular exchange between the delivery system and the body. Drug eluting coatings often incorporate powerful anti-proliferative drugs that are not intended for

release over long periods of time and thus slow unintended release of such drugs presents a potential risk to patients. In general, polymeric medical device materials contain small and potentially hazardous molecules and the potential that such molecules may leach into the body presents a serious public health concern. Potential leachables of concern include chemical additives (e.g. plasticizers and colorants) and byproducts of manufacturing (e.g. bisphenol-A<sup>5</sup>). Assessment of cumulative patient exposure to leachables over time requires knowledge of the diffusion rate of a specific leachable through a specific device material. Knowledge of diffusion rates for such systems would allow for an assessment of the relevant leaching timescales, which can persist for months, years, or decades. Knowledge of diffusion rate is also essential to assessing the timescale of ingress of

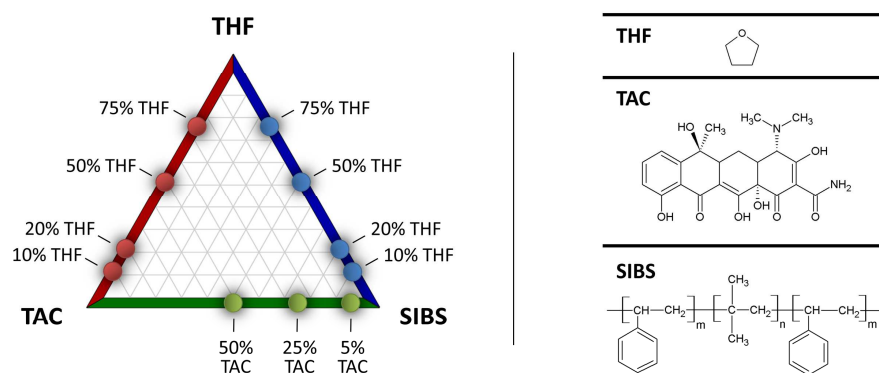


**Figure 1.** Chemical constituents (left) and ternary composition map (right) of simulated drug eluting stent coating. Drug = tetracycline (TAC); polymer = poly(styrene-*b*-isobutylene-*b*-styrene) (SIBS); solvent = tetrahydrofuran (THF). Limited solubility of drug/polymer effectively reduces the system to the 3 binary systems along the edges of the composition map. Simulations were performed for compositions indicated. Binary systems are distinguished by color in a manner consistent with color coding in Table 1: TAC/THC (red), SIBS/THC (blue), TAC/SIBS (green).

small molecules into polymeric device materials, which can adversely affect device safety. Water ingress into coatings on pacemaker leads and cochlear implants must, for example, be sufficiently slow to prevent electrical short-circuiting over the lifetime of the implant.

While ingress and egress of harmful molecular species have a direct and evident impact on device safety, diffusion affects device performance and reliability in more subtle but important ways. The drug release profile of drug eluting coatings depends on the specific drug/polymer microstructure formed during processing. Coating manufacture typically involves non-equilibrium processes, such as solvent casting, in which macroscopic phase separation is inhibited. Consequently, non-equilibrium microstructural features, such as drug inclusions, arise and the size and distribution of these features are dictated by diffusivity.<sup>6</sup> Such non-equilibrium microstructural features, along with other microstructural features, *e.g.* the presence of a drug wetting phase and the microphase-separated morphology of block copolymer components,<sup>7</sup> can profoundly impact drug release.<sup>8, 9</sup>

Thus, the safety and manufacturing reliability of next-generation drug delivery systems will all rely on the ability to accurately predict or measure molecular diffusivity for such systems. Unfortunately, experimental measurement of the slow diffusion of small to medium sized molecules in polymeric systems at physiological temperature, presents a significant challenge. This challenge is rooted in both the small size of the diffusants of interest and the inherently slow rate of transport in polymers.

Labelling techniques, most notably fluorescence recovery after photo-bleaching (FRAP), have been employed to study diffusion of large molecules, such as synthetic polymers,<sup>10-12</sup> polyelectrolytes,<sup>13</sup> proteins,<sup>14</sup> and dextrans.<sup>4</sup> However, fluorescence techniques are of limited utility in quantifying diffusivities of smaller molecules through polymeric and other highly viscous matrices; when a fluorescent labeling molecule is comparable in size to the diffusing molecule to which it is bound, the resulting complex is of significantly greater size

than the diffusing molecule alone, thus substantially altering the measured diffusion rate. Thus, applications of fluorescent labelling to the study of small molecule diffusion tend to focus on qualitative trends in diffusivity as a function of physico-chemical system characteristics. Examples include the effect on diffusion rate of probe size<sup>10, 15</sup> and charge,<sup>16</sup> the extent of hydrogen bonding between the probe and the polymer matrix, as well as the degree of stiffness,<sup>13, 17</sup> crosslinking density,<sup>18</sup> and hydrophobicity of the polymer matrix.

Extraction methods and approaches based on diffusion cells, which monitor increasing diffusant concentration in solution, are widely employed to measure small molecule release from polymeric materials. However, extraction approaches are of limited effectiveness where diffusion is slow and diffusant solubility in the extraction solvent is low, as is often the case for leachables in polymeric medical device materials. In this case, in order to release detectable quantities of diffusants in a reasonable timeframe, exhaustive extraction techniques using elevated temperatures and aggressive solvents must be employed. While exhaustive extraction is an important tool for determining the total amount of a contaminant in a device, it is of limited relevance to prediction of *in vivo* exposure.

Nuclear magnetic resonance (NMR), in particular pulsed field gradient spin echo (PGSE-NMR), has been used to determine diffusivity in solvent-rich systems, such as polymer solutions and gels.<sup>19-21</sup> However, in addition to being both costly and time-intensive, diffusion rates measurable by PGSE-NMR are limited to values greater than  $O(10^{-9})$  cm<sup>2</sup>/s and therefore may not be suitable to address health concerns discussed above, *e.g.* slow leaching of drugs or harmful molecules from devices.

Our work is focused on predicting diffusion of molecules larger than gases but relatively small on the scale of polymers (*i.e.* molecules with dimensions in the range of a few Angstroms to tens of Angstroms and molecular weights of approximately 50-1000 Daltons), which we will refer to as non-gaseous small molecules. Given the significant challenges in measuring non-gaseous small molecule diffusivity in polymers, it is of interest to explore the possibility of predicting diffusivity *in silico*.

Molecular dynamics simulation, a powerful computational tool that provides atomistically<sup>22</sup> detailed data on the motion of molecules in thermalized systems, is in principle an ideal approach to determining diffusivity. The quantitative relationship between diffusivity and individual molecular displacement was originally derived by Einstein<sup>23-25</sup> and can be expressed as

$$D = \frac{1}{6} \lim_{\Delta t \rightarrow \infty} \frac{d}{dt} \sum_{i=1}^{N_a} \langle |\mathbf{r}_i(t_o + \Delta t) - \mathbf{r}_i(t_o)|^2 \rangle \quad (1)$$

where  $i$  is the molecular index,  $N_a$  is the number of molecules in a given system,  $\mathbf{r}_i$  is the instantaneous three-dimensional position vector of molecule  $i$ ,  $t_o$  is an arbitrary reference time,  $\Delta t$  is the time differential over which squared displacements are computed, and the brackets  $\langle \rangle$  denote the ensemble average over multiple instances of the same chemical system. The summation in Equation (1) gives the mean-squared displacement of a given chemical species in a given system,  $\langle \Delta r^2 \rangle$ , for a given  $\Delta t$ . For sufficiently large  $\Delta t$ , the derivative of the mean-squared displacement is constant and thus  $D$  is independent of  $\Delta t$ . Equation (1) provides a straightforward method to determine diffusion coefficients directly from the trajectory output of simulation runs.

Molecular dynamics simulation has long been used to investigate molecular diffusion. Early work was restricted to qualitative studies of diffusion in coarse-grained<sup>26-28</sup> and simple fluid<sup>29, 30</sup> systems. With improvements in molecular mechanical force fields and dramatic increases in processor speed, diffusion studies have begun to address more complicated systems.<sup>31-38</sup> While a great deal of effort has focused on studying qualitative transport behavior of coarse-grained polymer systems,<sup>37, 39-42</sup> accurate predictions of diffusion in polymers using atomistic molecular dynamics simulation have been largely restricted to a few particularly small gases.<sup>43-55</sup> Obtaining accurate predictions of non-gaseous small molecule diffusivity at physiologic temperature in polymers remains a daunting challenge. In particular, published predictions of the diffusion in polymers of condensable vapors,<sup>55-57</sup> liquids,<sup>58-64</sup> drugs,<sup>65</sup> *etc.*, where available, are typically lacking in experimental validation and performed at highly elevated temperatures.<sup>53, 66-70</sup> A notable exception is work by Li *et al.*,<sup>71</sup> which stands to date as the most extensive and systematic comparison of simulation predictions and experimental measurements of diffusivity of small non-gaseous molecules in various polymers. Notably, simulation predictions for most diffusant/polymer systems were much larger than corresponding experimental values, by as many as four orders of magnitude.

This poor predictive performance is particularly surprising given that the simulation approach of Li *et al.* was substantially equivalent to the approach long applied successfully to gaseous diffusion in polymers. Furthermore, diffusants considered by Li *et al.* were limited to small or medium sized molecules and thus represented only an incremental increase in size over gas molecules. In this work, we present results that represent the first accurate and experimentally validated computational

predictions of small non-gaseous molecule diffusion in a polymeric system. In addition, we explore the physical basis underlying previous inaccurate predictions of molecular diffusion and suggest how simulations may be better applied to making meaningful predictions of transport in similar systems.

We model an important drug delivery system, polymer-based drug eluting stent (DES) coatings, which are commonly applied to implantable stents by casting drug and polymer from solution. DES coatings are essentially ternary drug/polymer/solvent systems where composition changes over the lifetime of the coating, as solvent evaporates during casting or as drug is released *in vivo*. Our simulated DES system is represented by the composition map shown in Figure 1 and includes the following components: poly(styrene-*b*-isobutylene-*b*-styrene) (SIBS) tri-block copolymer, widely employed in commercial DES coatings; tetrahydrofuran (THF), commonly used in solvent casting of DES coatings; and tetracycline (TAC), an antibiotic drug that is not employed in DES coatings, but serves as a safe surrogate drug for our accompanying laboratory work and is comparable in size and chemical structure to the powerful and often toxic drugs used in DES coatings. Due to chemical incompatibility of polymer and drug, the system can be well understood by considering only binary systems of solvent-polymer, solvent-drug, and drug-polymer, *i.e.* the three binary axes of the ternary composition map shown in Figure 1. In this work, we predict diffusion constants at the compositions along each of these binary axes shown in Figure 1. Knowledge of diffusivity values at these compositions will provide essential quantitative insight into chemical transport rates within drug eluting coatings throughout the entire product life cycle. For example, predicted drug diffusivity in SIBS can be used in conjunction with film thickness and morphology to predict order of magnitude release times for embedded drug and/or residual solvent. Furthermore, predicted diffusion coefficients presented herein serve as the basis for hierarchical predictive modeling by providing parameters necessary for meso- and macro-scale models. In particular, diffusivity values are a necessary prerequisite for our ongoing phase field modeling studies<sup>72</sup> of entire product life cycle of drug eluting stent coatings, from microstructure formation during processing to subsequent release.

## Methodology

### Simulation

Initial amorphous structures were constructed using Materials Studio software from Accelrys based on the approach of Theodorou and Suter<sup>73</sup>. Molecules were grown incrementally such that the ensemble-distributions of chain torsions in the completed structure are consistent with those found in equilibrium mixtures. Growing chain configurations were also checked for high energy close-contacts and un-physical ring sparring configurations, which were discarded from consideration. Initial structures were constructed at lower density (0.4 g / cm<sup>3</sup> to 0.6 g / cm<sup>3</sup>) and subsequently ramped to density 0.84 g / cm<sup>3</sup> using an alternating series of molecular

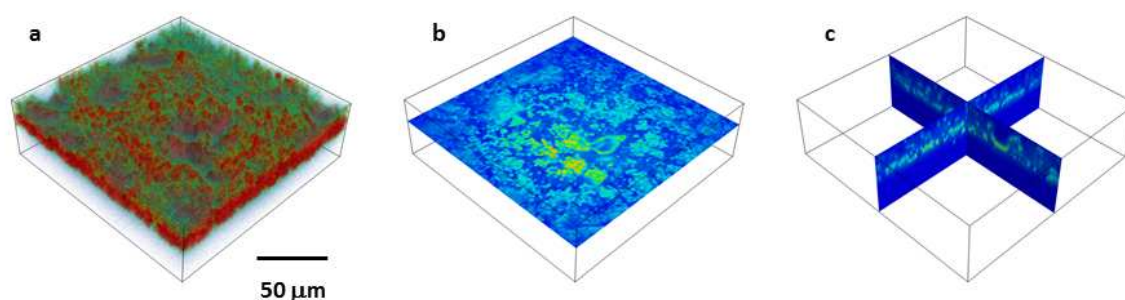


Figure 2. Confocal Microscope Images of Drug Microstructure in Drug/Polymer (TAC/SIBS) Coating. High drug concentration is indicated by red in (a) and light green in (b) and (c). Three-dimensional data shown in (a) demonstrate lamellar distribution of drug within the coating. Drug distribution along a single plane within the drug-rich lamellar layer is shown in (b). Perpendicular cross-sections along the depth of the coating are shown in (c). Drug distribution within the coating is consistent with a second-rank laminate model.

dynamics steps and geometry optimization. Structures were then subjected to additional energy-minimization using an alternating sequence of steepest descent and conjugate gradient optimizations to an energy tolerance of 0.01 kcal / mol. To expedite calculation of electrostatic interactions during construction of initial amorphous cell structures, charge groups, in which individual charges for a group of atoms are consolidated onto a single center, were employed. Assignment of charges was performed based on the 'subunit' assignment method of Materials Studio and cutoff distances of 10 Å and 8 Å were utilized for Lennard-Jones and electrostatic interactions, respectively.

In total, 57 amorphous structures were generated (including multiple versions of each binary system and concentration shown in Figure 1) in Materials Studio and exported for subsequent density equilibration and production runs. Production runs were performed using LAMMPS<sup>74</sup>, open source software made available by Sandia National Laboratory. The generalized Amber force field (GAFF)<sup>75</sup> was employed for molecular dynamics simulation runs in LAMMPS. GAFF is designed to provide realistic interactions between different types of molecules - *e.g.* drug and polymer - that are not treated by traditional force fields. A handful of torsion parameters for our system were missing and were determined from available parameters as prescribed in Wang *et al.*<sup>75</sup>

Initial structures imported to LAMMPS from Materials Studio were each subjected to a six million step equilibration in the isobaric-isothermal (NPT) ensemble to eliminate remaining high energy structural features and to determine equilibrium density for subsequent production runs in the canonical (NVT) ensemble. A time-step of 1 fs was utilized for the first 2 million steps of the isobaric-isothermal equilibration runs, followed by 4 million time-steps of 4 fs each. Density for a given binary system at a given concentration was determined by averaging the density of all individual runs over the final 1 million steps. In the final stage prior to production runs, the box size for each individual run was linearly ramped over 100,000 steps to attain

the appropriate average density determined in the isobaric-isothermal stage.

Production runs utilized a time-step of 4 fs, such that a total of 250,000,000 steps were required to achieve 1 μs of simulation time. Center-of-mass trajectories for individual drug, polymer, and solvent molecules were sampled every 10 picoseconds. Our simulated system was fully atomistic and the vibrational motion of hydrogen atoms was explicitly considered, as employing the SHAKE algorithm to hold bond lengths of H-atoms fixed had a surprisingly large effect on system dynamics. A cutoff distance of 12 Å was utilized for both Lennard-Jones and electrostatic interactions.

Simulations were run in parallel with 24 to 48 processors dedicated to individual runs. The amount of wall required to complete the simulation runs was large (of the order of months) and the total processor time, (total wall time)\*(#processors/run)\*(#runs), for our set of simulations was very large, as documented in Table I.

### Experimental

To validate our simulation predictions, films of SIBS were cast from THF and utilized for vapour sorption analysis (VSA) diffusivity determinations. Films of SIBS tri-block polymer (30 wt % polystyrene) were fabricated by solution casting into fluorinated polymeric moulds from 5 % (w/v) THF. After drying in air for 12 hours, the films were removed from the moulds and placed under vacuum at 1 Torr for 48 hours. The entire drying procedure was conducted at room temperature and resulted in polymer films of  $\approx 60$  μm thickness. The dried films were then placed in a vapour sorption analyser. After equilibration at 37 °C, THF mass uptake was measured as a function of time at five different solvent partial pressures or activities, *a*, until equilibrium was achieved. The binary diffusion coefficient,  $D_{sp}$ , and the solvent concentration, *C*, at each of the five activities was determined by fitting mass uptake data to the one-dimensional analytical solution to Fick's second law<sup>76</sup>,

$$\frac{M_t}{M_{eq}} = 1 - \frac{8}{\pi^2} \sum_{n=0}^{\infty} \frac{1}{(2n+1)^2} \exp\left[\frac{-D(2n+1)^2\pi^2 t}{L^2}\right] \quad (2)$$

where  $M_t$  is the mass at time  $t$ ,  $M_{eq}$  is the mass at equilibrium, and  $L$  is the coating thickness. To facilitate a direct comparison with the molecular dynamics predictions, the best fit diffusion coefficients were converted to THF self-diffusivity using an established method.<sup>77</sup> The procedure described above was repeated five times and the resulting standard deviations in  $D_{sp}$  were less than 50% of the average values.

In theory, the same approach could be utilized to determine the THF diffusivity as function of concentration in TAC. In practice, however, challenges arise associated with fabricating macroscopic films of TAC (required by vapor sorption methods) that are both structurally sound and consistent with the microscopic phases present in thin drug-polymer composite coatings. Pure TAC coatings manufactured by this method do not fully densify and therefore are extremely brittle and prone to cracking; thus, solvent uptake is dictated not by the intrinsic behavior of the material but by the pore space. To circumvent these issues, composites coatings of TAC and SIBS (with varying TAC concentrations of 0.8, 0.12, 0.16 w/w) were fabricated. THF uptake into these composite coatings was determined using the same approach described above, allowing for a determination of the effective THF diffusivity,  $D_e$ , within the composite. From the effective diffusivity in the composite, we were able to determine the THF diffusivity in the drug phase using the following procedure.

We note that the structure of the composites, as exemplified in confocal images provided in Figure 2, is representative of a second rank laminate.<sup>78</sup> Images were collected using a Leica (Solms, Germany) TCS SP-2 confocal microscope. This structure is consistent both with previous reports of microstructures in spray cast TAC-SIBS composite coatings<sup>6</sup> and computer simulations of spray cast structures.<sup>9, 72</sup> A second rank laminate structure consists of alternating layers parallel to the film surface consisting of either pure polymer (1) or drug and polymer (2). For this configuration, the relationship between the diffusivity of the ensemble  $D_e$  perpendicular to the film surface and the diffusivities of the layers  $D_i$  is given by,

$$D_e = \frac{D_1 D_2}{D_2(1-\phi) + D_1\phi} \quad (3)$$

where  $\phi$  is the volume fraction of layers with both drug and polymer. The structure within these drug-polymer layers is further assumed to consist of alternating layers of drug and polymer that are perpendicular to the top level layers. Thus, within these layers we have:

$$D_1 = D_{sp}(1-\Phi) + D_{sd}\Phi \quad (4)$$

where  $D_{sp}$  and  $D_{sd}$  are the diffusivities of solvent (THF) in the pure polymer (SIBS) and pure drug (TAC) phases, respectively, and  $\Phi$  is the volume fraction of the pure drug within the drug-

polymer layers. To progress, we recognize that  $\phi$  and  $\Phi$  are related through the total volume fraction of drug in the ensemble,  $V_d = \phi\Phi$ . We note that in the limits of  $\Phi=1$  and  $\phi=1$ , there exist only layers of pure drug and pure polymer, perpendicular and parallel to film surface, respectively. Thus, the model encompasses a range of potential structures including the extrema.

After introducing the above constraint, Equation (3) can be expressed as:

$$\frac{D_e}{D_{sp}} = \frac{1 + \Phi(R-1)}{1 + (\Phi - V_d)(R-1)} \quad (5)$$

where  $R$  is the ratio of binary diffusion coefficients  $D_{sd}/D_{sp}$ . Based on the measurements described above, we have determined values of  $D_e/D_{sp}$  at five different activities and three values of  $V_d$ , for a total of 15 equations. Further,  $R$  depends only on activity and the microstructure parameter  $\Phi$  depends only on  $V_d$ . Thus, we have at most eight unknowns and an overdetermined system of equations. Here, we have further assumed that the topology of the structure is invariant, *i.e.*  $\Phi$  is constant over the range of  $V_d$  probed, reducing the number of unknown parameters to six. This simplification was made after observing that the fit values of  $\Phi$  did not vary substantially when they were solved for separately. Therefore, based on

(5), we determined the ratio  $D_{sd}/D_{sp}$  and  $R$  at each of the five activities, as well as the structural parameter  $\Phi$ , using a standard non-linear least squares routine. Standard errors in the fits for  $D_{sd}/D_{sp}$  were less than 20% of the fit values. We note that the application of

(5) assumes that the solvent solubility in both the drug and polymer phase of the composites are identical. In fact, there was no discernible difference between  $C(a)$  measured in SIBS compared to any of the composite structures. Thus, the  $C(a)$  determined for SIBS was used to convert the fit  $D_{sd}$  values to the THF self-diffusivity in TAC using the previously referenced approach<sup>79</sup>.

## Results and Discussion

A summary of our simulated systems and predicted diffusion coefficients is provided in Table I. Results are categorized most broadly by the chemical identity of the binary system, *i.e.* THF/TAC, THF/SIBS, and TAC/SIBS. Each row of data summarizes simulations for a specific binary system at a fixed concentration, for which there are multiple independent runs. Data provided in the table include the number of independent runs, the simulation time ( $\Delta t_{sim}$ ) per run, the total processor time expended for all runs for a given binary system at a given concentration ( $t_{proc}$ ), system density ( $\rho$ ) employed in the production run, the number of atoms per simulation box ( $N_{atoms}$ ), the length of the simulation box ( $L_{box}$ ), the characteristic length scale of confinement of Hydrogen atoms in the system (the Debye-Waller factor,  $u^2$ ), and predicted diffusion coefficients,  $D_{pred}$ , with standard deviation.  $D_{pred}$  values are provided for both TAC and THF diffusivity.  $\Delta t_{sim}$

equals the number of molecular steps per run multiplied by the temporal increment of each time-step.  $t_{\text{proc}}$  equals the total elapsed wall time multiplied by the number of processors

employed for a given run summed over all runs. In total, 57 independent simulation runs, each of approximately one  $\mu\text{s}$  in duration, were performed. Simulations of this

	conc.	# runs	$\Delta t_{\text{sim}}$	$D_{\text{pred}}^{\text{THF}}$	$D_{\text{pred}}^{\text{TAC}}$	$\rho$	$N_{\text{atoms}}$	$L_{\text{box}}$	$\langle u^2 \rangle$	$t_{\text{proc}}$
	[weight %]		[ns]	[ $\text{cm}^2/\text{s}$ ]	[ $\text{cm}^2/\text{s}$ ]	[ $\text{g}/\text{cm}^3$ ]		[Å]	[Å <sup>2</sup> ]	[yrs]
THF / TAC	10% THF	4	1016	3.4e-9 (1.5e-9)	8.8e-11 (6.1e-11)	1.24	1371	26.6	3.7	10.2
	20% THF	5	1018	3.0e-8 (2.3e-8)	4.8e-10 (2.3e-10)	1.21	1303	25.8	4.9	12.3
	50% THF	6	1020	2.8e-6 (3.6e-7)	1.8e-7 (6.0e-8)	1.06	1232	24.4	9.8	14.3
	75% THF	5	986	1.1e-5 (2.4e-6)	1.7e-6 (9.7e-7)	0.95	1186	23.8	12.0	15.3
THF / SIBS	10% THF	5	1038	1.1e-8 (9.2e-9)	-	0.90	1565	24.2	2.3	11.2
	20% THF	5	1142	8.1e-8 (4.6e-8)	-	0.90	1747	25.1	3.1	17.6
	50% THF	3	1037	3.7e-6 (2.1e-7)	-	0.89	1819	25.7	8.1	13.0
	75% THF	4	1213	1.2e-5 (2.8e-6)	-	0.86	1774	26.3	12.8	10.3
TAC / SIBS	5% TAC	7	1024	-	4.2e-11 (6.1e-11)	0.89	1478	23.9	0.7	17.1
	25% TAC	7	1019	-	2.9e-11 (1.1e-11)	0.95	1702	25.6	0.8	14.4
	50% TAC	6	1024	-	2.7e-11 (2.1e-11)	1.05	1564	25.8	0.80	15.4

Table 1. Overview of simulated systems and predicted diffusion constants.

duration remain computationally demanding and greater than one hundred years of total processor time were expended in running the entire set of simulations.

It is instructive to compare overall trends in our predicted diffusion coefficients to those of Li *et al.* Whereas experimental values of diffusion coefficients tabulated by Li *et al.* varied widely as a function of system composition, from roughly  $10^{-5} \text{ cm}^2 / \text{s}$  to  $10^{-9} \text{ cm}^2 / \text{s}$ , simulation predictions for the same systems were heavily biased towards the more rapid end of the range, from roughly  $10^{-5} \text{ cm}^2 / \text{s}$  -  $10^{-7} \text{ cm}^2 / \text{s}$ . Notably, simulation predictions of reasonable accuracy, *i.e.* predictions of the same order of magnitude as the corresponding experimental values, corresponded to the fastest diffusing systems, whereas the most erroneous predicted values corresponded to systems for which the experimentally determined diffusion was slowest. The experimental diffusivities tabulated by Li *et al.* clearly trend towards slower diffusion for systems with larger diffusants and less flexible polymers, whereas faster diffusivity was characteristic of systems featuring smaller diffusants or polymer backbones with higher degrees of flexibility. Taken together, this strongly suggests that poor diffusivity prediction was largely attributable to the inability to accurately predict slower diffusion in systems with more restricted dynamics and that it is important to be mindful of the potential to overestimate diffusion rates for systems of more limited mobility.

Encouragingly, our predicted diffusion constants,  $D_{\text{pred}}$ , are strongly system dependent in a manner more consistent with experimental results,<sup>65, 80</sup> spanning orders of magnitude with chemical composition. The upper limiting values of our  $D_{\text{pred}}$  values extend to nearly  $10^{-5} \text{ cm}^2 / \text{s}$  for THF diffusion in systems with high THF concentration. For a given binary system containing THF, the higher the THF concentration, the

more fluid-like, or the less constrained the dynamics. Our lowest  $D_{\text{pred}}$  estimates are of the order of  $10^{-11} \text{ cm}^2 / \text{s}$  and correspond to diffusion of the larger drug molecule TAC in the polymer SIBS in the absence of THF.

While observed trends between our  $D_{\text{pred}}$  values and system composition are encouraging, to demonstrate the accuracy of our simulation predictions requires validation with experimental measurements on the same system. As discussed in the introduction, experimental determinations of diffusivity of small non-gaseous molecules in polymer systems is highly challenging, particularly for systems where diffusivity is particularly slow, *e.g.* systems of low solvent concentration. While it is not feasible to experimentally validate predicted diffusion constants for all, or even most, system compositions and concentrations treated in our simulation work, it is particularly important to have validation at low solvent concentration. Such systems are most relevant to concerns related to leaching and are the most challenging to accurately predict using molecular dynamics simulation.

To provide such validation, we have employed vapor sorption analysis (VSA) to measure the diffusive uptake of THF vapor into films of polymer and drug. THF mass in the coating was measured as a function of time over a range of THF activities and fitted to the analytic solution to Fick's second law in one-dimension. Mutual coefficients determined in this way were subsequently converted to self-diffusion coefficients using the method of Duda *et al.*<sup>77</sup> to allow for direct comparison with our molecular dynamics predictions. Weight fraction of THF was determined by subtracting the original film mass from the mass following THF uptake and equilibration. Details of the VSA technique and our composite film approach to determining THF diffusion in TAC are provided in the Experimental Methods section.

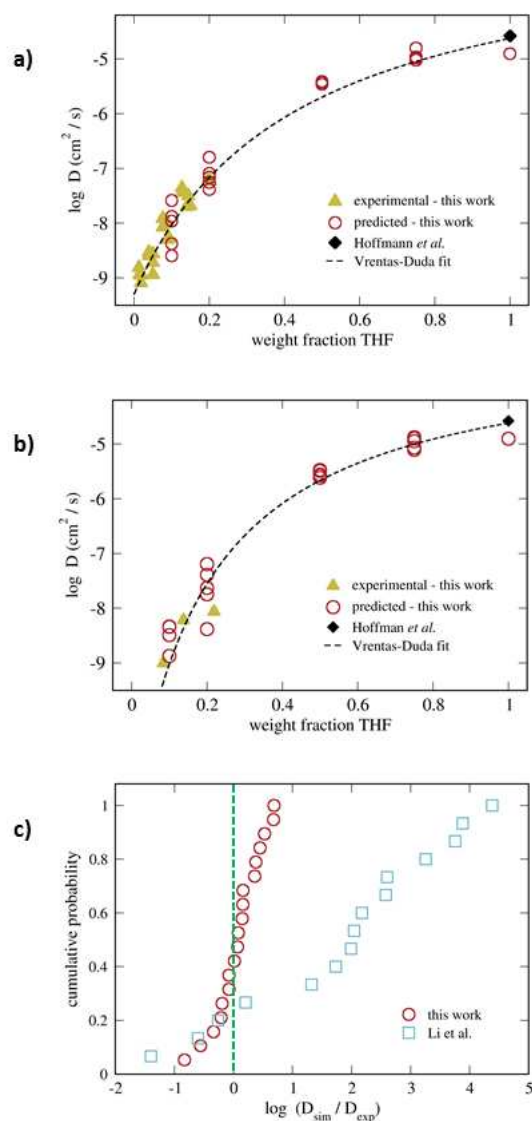


**Figure 3.** Comparison of predicted and experimental diffusion coefficients. Predicted (simulation) and experimental (vapor sorption) diffusion coefficients for THF diffusion in SIBS (a) and TAC (b). The literature value for THF self-diffusion is included for comparison (solid black diamond). For (a), experimental data shown correspond to individual measurements. Uncertainty in experimental data for (b) is discussed in Experimental Methods. (c) Discrete cumulative probability comparison of predicted ( $D_{\text{sim}}$ ) vs. experimental ( $D_{\text{exp}}$ ) diffusion coefficients for this study (red) and the work of Li *et al.* (blue).

While VSA measurements are limited to systems with volatile diffusants, we were able to use VSA to validate our simulations along two of the THF-containing binary axes (THF/TAC and THF/SIBS) of our model system composition map shown in Figure 1. While VSA experiments are further limited to low solvent concentration within the coating (to maintain mechanical integrity of the coating) literature values for self-diffusion in pure THF provides validation at the upper bounds of the THF/TAC and THF/SIBS axes. At the conclusion of this work, we will address the reasonableness of our drug diffusion predictions, which cannot be validated with VSA.

In Figure 3, predicted (simulation) and experimental (VSA) diffusion coefficients of THF in SIBS (Figure 3a) and THF in TAC (Figure 3b) are plotted as a function of THF mass fraction. Multiple determinations of diffusivity were made at each of THF concentration and data points in Figure 3a and Figure 3b correspond to individual determinations. For systems with low THF concentration (10% THF and 20% THF),  $D_{\text{pred}}$  values for THF fall in the range from  $10^{-8} \text{ cm}^2/\text{s}$  to  $10^{-9} \text{ cm}^2/\text{s}$ . Agreement with experimental VSA values is impressive, particularly given that the predictions of Li *et al.* were poorest when compared to experimental diffusivities in this range. Furthermore,  $D_{\text{pred}}$  for pure THF,  $1.2 \times 10^{-5} \text{ cm}^2/\text{s}$ , is in good agreement with literature values<sup>81</sup> for THF self-diffusion ( $2.6 \times 10^{-5} \text{ cm}^2/\text{s}$ ). A fit to all data based on the well-known Vrentas-Duda model<sup>79,82</sup> of diffusion, which has been shown to provide good empirical fits to small molecule diffusion in polymers as a function of solvent concentration, is also shown in Figure 3. While no experimental data are available for 50% THF and 75% THF systems, there is good agreement between predicted diffusivities and the Vrentas-Duda model fit.

In Figure 3c, a discrete cumulative probability distribution plot is shown, providing a visually intuitive means of quantifying order of magnitude deviations between our predicted and experimental data. The cumulative distribution function,  $C_x$ , of a real valued random variable  $X$  is given by

$$C_x(X) = P(X < x) \quad (6)$$

*i.e.* the probability that the random variable  $X$  takes on a value less than  $x$ . For our purposes, the random variable  $X$  is taken from the set of  $\log(D_{\text{pred}}/D_{\text{exp}})$  values obtained by comparing each  $D_{\text{pred}}$  value from an independent simulation run to the corresponding average experimental value for the same system. Thus, the more clustered the cumulative probability distribution values are around  $\log(D_{\text{pred}}/D_{\text{exp}}) = 0$ , the more accurate are the set of predictions. (As experimental values do not correspond precisely to the same THF concentrations at which simulation predictions were performed, experimental values were interpolated from the Vrentas-Duda fit to all data shown in Figure 2a and Figure 2b.) Our predicted values can be seen to fall well within an order of magnitude of experimental values with no apparent bias towards over-prediction or under-prediction of experimental values. Furthermore, the cumulative probability distribution shown in Figure 2c tends to understate the predictive accuracy of our simulations, as calculated from individual runs at a given concentration, rather than as an average over multiple runs. The cumulative probability distribution for the predictions of Li *et al.* is also shown in Figure 2c, illustrating a strong bias towards over-prediction of diffusion coefficients.

We now turn to a discussion of the basis for our improved diffusivity predictions and offer insight into how to avoid inaccuracy in simulation predictions of diffusivity. The accuracy of molecular dynamics simulations depends in part on how accurately interatomic and intra-molecular potentials

represent the forces acting between constituent atoms in a simulated system. The choice of force field and its suitability for given system is widely recognized as a potential source of error. However, other considerations can strongly affect the accuracy of calculated system properties. Condensed soft matter systems feature complex time-dependent dynamics and entropy effects that must be properly treated for meaningful simulation results. We have previously demonstrated that neglect of intra-molecular configurational entropy and molecular flexibility in molecular mechanics based docking studies can profoundly impact predicted binding strength independent of choice of force field.<sup>83</sup> Similarly, we have previously shown that simulation of viral ds-DNA genome packing into capsids depends upon molecular relaxations within the crowded capsid.<sup>84</sup> In order to properly predict the experimentally observed features of genome packing, simulations must utilize constant packing force, rather than constant packing velocity to allow for time-dependent relaxations to occur. In both cases, the improper treatment of system dynamics results in significant error.

The key insight underlying our greatly improved simulation predictions of diffusivity relates to recognizing the fundamental difference in diffusive mechanisms of small non-gaseous molecular diffusion *vs.* gaseous diffusion in condensed systems, in particular the dependence of small non-gaseous molecule diffusion on the constrained dynamics of the molecular matrix through which diffusion occurs.

Numerous simulation studies of diffusion of small gases in polymers have suggested that diffusion occurs via activated 'hopping' of gas molecules amongst the existing free volume elements within a polymer.<sup>54, 85, 86</sup> Hopping is facilitated by vibrations and highly-localized segmental motions of polymers in the surrounding matrix, which open up momentary pathways between existing free volume elements. Because this mechanism of diffusion is independent of structural relaxations<sup>87</sup> and depends only on high frequency highly localized dynamics of the polymer matrix, simulations of gas diffusion have successfully utilized simulation times as short as tens of ps.

However, experimental work of Mohamed *et al.*<sup>88</sup> and simulation work on gas diffusion through polymers<sup>54, 87</sup> have both demonstrated that even gas diffusion is dependent to some extent upon relaxational dynamics of the surrounding polymer matrix: for all but the smallest gas molecules, diffusion cannot occur when polymer motion is restricted to vibrational fluctuations around an equilibrium configuration, but rather requires at least some degree of local rearrangement of surrounding polymer molecules. This strongly suggests that the hopping model is not suitable to describe diffusion of molecules larger than gases (e.g., condensable vapors, liquids, drugs), which are too large to fit within or to jump between existing free volume elements. Rather, diffusion of such molecules must be facilitated by larger scale coordinated segmental rearrangements, or relaxations, of the surrounding molecular matrix, whose characteristic timescales significantly exceed those of vibrational motions.

Thus, despite representing only an incremental increase in molecular size over gas molecules, small non-gaseous molecules likely diffuse via a fundamentally different mechanism reflecting the time-dependent dynamics of the surrounding molecular matrix. Molecular displacements will exhibit time-dependence related to the timescale over which diffusion-enabling relaxations occur in the matrix, which in turn depends on the glassiness of the matrix.

Numerous aspects of our  $D_{\text{pred}}$  data provide evidence for the relaxation-dependent diffusion mechanism that has been hypothesized. First,  $D_{\text{pred}}$  values were found to increase when the solvent concentration of a given system increases. The presence of solvent reduces system glassiness and thus diffusivity should increase with increasing THF concentration for THF-containing binary systems, (i.e. THF/SIBS and THF/TAC). The  $D_{\text{pred}}$  values for the THF/TAC and THF/SIBS systems in Table I are indeed consistent with this expectation: diffusivity values for both THF and TAC increase by roughly an order of magnitude with each increment in THF concentration (i.e. from 10% to 20% THF, from 20% THF to 50% THF, and from 50% THF to 75% THF).

Second, diffusivity of the larger diffusant TAC was found to be generally slower than diffusivity of the smaller THF. Diffusivity should decrease with increasing diffusant size as larger diffusants require larger scale and thus significantly slower relaxations to accommodate transport. For TAC/THF systems, THF diffusivity is roughly one to one and a half orders of magnitude faster than TAC diffusivity at all THF concentrations. For the case of diffusion through SIBS, the effect of diffusant size is more difficult to isolate, as THF is not only smaller than TAC, but also enhances the system fluidity. Thus, we point to the 10% THF/ 90% SIBS system, for which THF diffusivity is roughly two orders of magnitude faster than TAC diffusivity in SIBS.

Third,  $D_{\text{pred}}$  values exhibit time-dependence reflecting the time-dependence of the diffusion-enabling relaxations of the surrounding molecular matrix. To explore the time-dependence of  $D_{\text{pred}}$  in our simulations, we have iteratively applied Equation (1) to determine  $D_{\text{pred}}$  for a series of  $\Delta t$  values ranging from  $\Delta t = 20$  ps to  $\Delta t = 500$  ns in increments of 20 ps. We note that  $D_{\text{pred}}$  for a given  $\Delta t$  is determined using Equation (1) by ignoring the necessary condition  $\Delta t \rightarrow \infty$ . While diffusion coefficients are properly time independent,  $D_{\text{pred}}$  is expected to be time dependent for sufficiently short times that the condition  $\Delta t \rightarrow \infty$  is not satisfied. Thus, any range of  $\Delta t$  for which  $D_{\text{pred}}$  is time-dependent indicates that corresponding  $D_{\text{pred}}$  values are not proper diffusivities but nonetheless provide a means to monitor the convergence of  $D_{\text{pred}}$  values to proper diffusivities.

In Figure 4a, resulting  $D_{\text{pred}}$  *vs.*  $\Delta t$  values are plotted for each of our simulated systems. In terms of the relaxation-based hypothesis of transport, we expect time-dependence of  $D_{\text{pred}}$  to occur at small enough timescales, reflecting the fact that diffusivity cannot accurately be determined at timescales less than the characteristic relaxation time of the surrounding molecular matrix. From Figure 3a, it is apparent that time

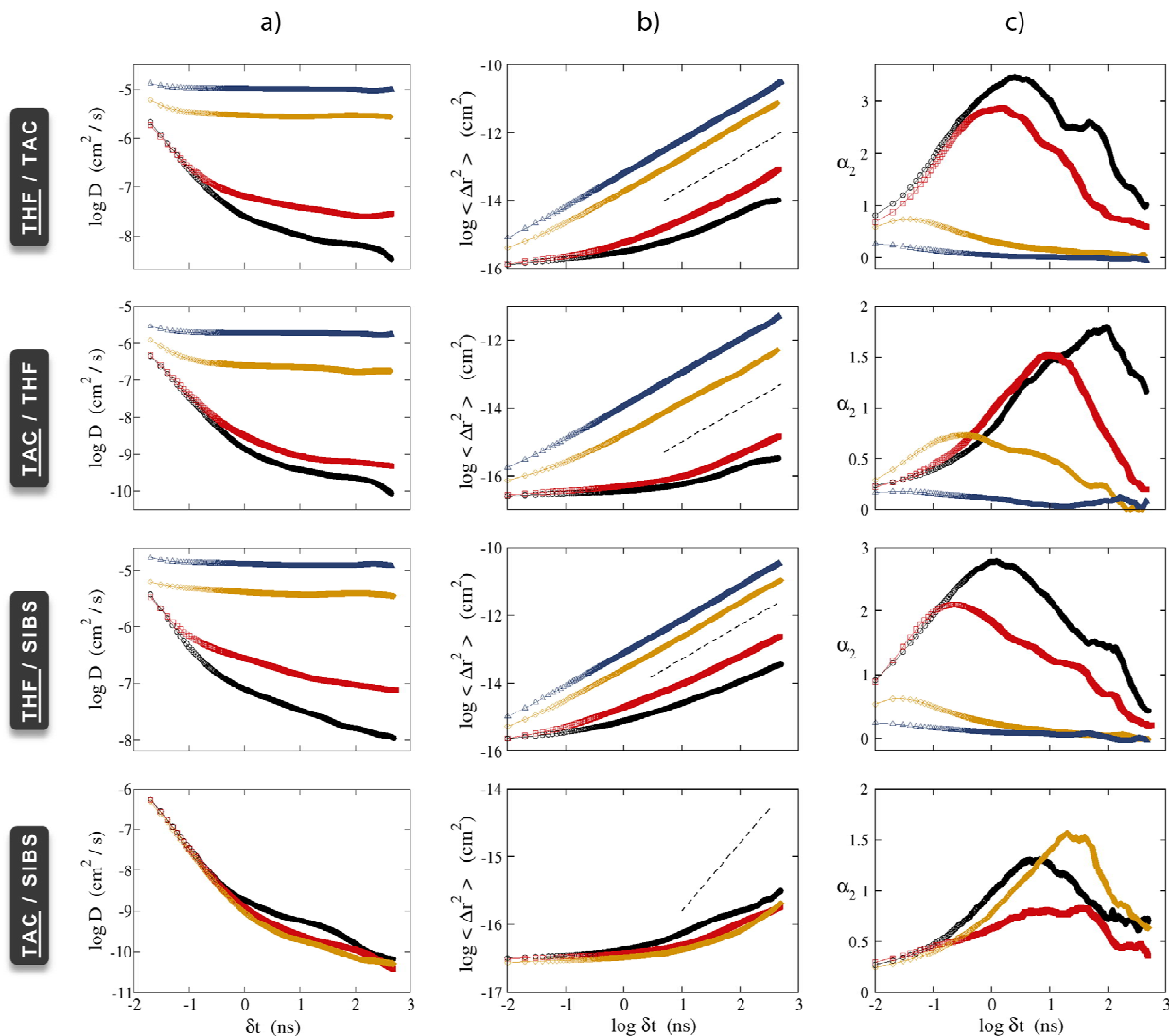


**Figure 4.** Time-dependence of diffusion behavior. Each row corresponds to a specific binary system, identified by the banner on the left, with the diffusing species underlined. THF concentrations are color coded as follow: 10% (black), 20% (red), 50% (gold), 75% (blue). For TAC/SIBS system, TAC concentrations are coded by color as follow: 5% (red), 25% (gold), 50% (black). (a) Dependence of calculated diffusion constants on simulation duration. (b) Log-log plot of ensemble average mean square displacement of diffusing species. The slope of the plot is equal to the exponent  $\alpha$ , from the relation  $\langle \Delta r^2 \rangle \sim \Delta t^\alpha$ . For the diffusive regime,  $\alpha=1$  (dashed line). (c) Non-Boltzmann parameter, a measure of non-Gaussian displacements, as a function of simulation duration.

dependence of  $D_{\text{pred}}$  is most pronounced at short times, progressively decreasing with increasing time and eventually converging asymptotically. Furthermore, the error in  $D_{\text{pred}}$  is largest and the time-dependence of  $D_{\text{pred}}$  persists over longer timescales for glassier systems where relaxations are more infrequent.

For example, for systems with little or no THF content (*i.e.* 10% THF / 90% TAC, 10% THF / 90% SIBS, and all SIBS / TAC systems),  $D_{\text{pred}}$  can be seen to exhibit a remarkable degree of time-dependence, decreasing by orders of magnitude over many orders of magnitude of time. As THF content is progressively increased for THF / TAC and THF / SIBS

systems, the magnitude and duration of error in  $D_{\text{pred}}$  correspondingly decrease. Systems with a high THF content and thus higher degree of fluidity exhibit minimal time-dependence of  $D_{\text{pred}}$ .

The time-dependence of  $D_{\text{pred}}$  values provides a simple explanation for how the same molecular dynamics simulation approach could have successfully been used to predict gaseous diffusion yet unsuccessfully applied to predicting small non-gaseous molecular diffusion. For systems with gaseous diffusants, convergence of  $D_{\text{pred}}$  occurs within tens of ps of simulation time. The typical simulation duration employed by Li *et al.* for predictions of diffusion in polymers was also of the order of tens of ps. However, for diffusion in low-solvent systems, Figure 3a illustrates that diffusivity is far from converged at this timescale. The smallest time considered in Figure 3a is 20ps, at which  $D_{\text{pred}}$  values are greatly overestimated for low-solvent systems. Taken together, the time-dependent behavior of  $D_{\text{pred}}$  strongly suggests that simulations of insufficient duration on glassy systems lead to large overestimations of diffusivity. The origin of the time-dependence of  $D_{\text{pred}}$ , and thus likely the source of large error in diffusivity predictions, can be traced to individual molecular motions, as illustrated in Figure 5, for which the trajectories of select THF molecules in simulated THF/SIBS systems are shown. Entire  $\mu\text{s}$  trajectories of individual molecules are shown in Figure 5a, with displacements at 10 ps intervals represented by a straight line. Such individual displacements, which are not distinguishable in Figure 5a, can be seen in the enlarged regions of the molecular trajectories shown in Figure 5b. For systems with lower solvent concentration (*i.e.* 10% THF and 20% THF systems), molecular trajectories become localized for extended periods, as is particularly evident in Figure 5b. The molecules are temporarily entrapped or ‘dynamically caged’<sup>32, 89</sup> by surrounding molecules until surrounding molecular segments undergo necessary collective motions to allow the diffusing molecule to escape. Individual caging events are terminated by brief punctuated bursts of displacement, after which a new caging event is initiated.

Due to the enhanced mobility of the surrounding molecular matrix, the dynamic caging phenomenon diminishes progressively with increasing THF concentration, as caging events gradually become indistinguishable from punctuated displacements and the trajectories approach a self-similar random walk. We can infer that displacements corresponding to caging events are non-Gaussian, as a series of Gaussian displacements give rise to a random walk. This relationship is illustrated in the rightmost column of Figure 5, where a random walk trajectory has been generated by drawing displacements from a Gaussian distribution centered at 0. For the rightmost column of Figure 5, length is given in units of  $\sigma$ , the standard deviation of the Gaussian distribution. The temporary caging of diffusing molecules constitutes a classic ‘dynamic heterogeneity’ in displacement,<sup>80, 90-93</sup> wherein non-Gaussian displacements dominate during the characteristic timescale of caging and Gaussian displacements predominate over longer timescales.<sup>91</sup> The dynamic caging exhibited by low THF

systems in Figure 5b is a hallmark of glassy or ‘sub-diffusive’ dynamics, which we previously hypothesized as the physical basis of the time dependence of  $D_{\text{pred}}$  shown in Figure 4a.

Step size distribution for THF diffusion in SIBS is shown in Figure 5c for a number of different sampling times and provides further evidence for the dynamic heterogeneity in displacement. For sufficiently small timescales, a single displacement peak is evident, centered at approximately 1 Å, which corresponds well with the size of the dynamic cages distinguishable in Figure 5b. This peak is attributable to the ‘rattling’ of THF within the dynamic cage. As sampling time increases, a smaller secondary peak emerges at larger displacement, attributable to less frequent but larger punctuated jumps between cages. As the timescale of sampling further increases, the peak representing rattling within an individual cage diminishes, but does not shift in displacement, while the peaks corresponding to inter-cage jumps become more pronounced and shifted to larger displacements, indicating that only the peaks at larger displacement correspond to diffusive motion.

As expected, THF concentration affects the timescale of the transition from predominantly short-range caged motion to larger scale Gaussian displacements. The appearance of the secondary peak indicates the initiation of diffusive displacements and occurs at progressively shorter timescales as THF concentration increases for a given system. For example, the secondary peak for the 10% THF / 90 % SIBS system is nearly indiscernible up until 250 ns. For the 50% THF / 50% SIBS systems, the secondary peak is evident by 100 ps. At 250 ns, intra-cage rattling and inter-cage jumps remain somewhat distinct only for the 10% THF / 90% SIBS system.

This interpretation of step size distribution in terms of onset of diffusive motion is consistent with the time-dependence of  $D_{\text{pred}}$  observed in Figure 4a, where the duration of the time-dependent sub-diffusive regime of  $D_{\text{pred}}$ , attributable to localized ‘rattling’ displacements, is shown to decrease with increasing THF concentration. We emphasize that non-Gaussian displacements dominant at short time are inconsistent with the assumption  $\Delta t \rightarrow \infty$  required for use of Equation 1 and therefore should lead to error in  $D_{\text{pred}}$  values for as long as such non-Gaussian displacements are dominant.

We have thus far presented evidence that sub-diffusive dynamics are present in our systems and can introduce very large in error  $D_{\text{pred}}$  values. Furthermore, Figure 4a and Figure 5c both suggest that sub-diffusive dynamics are present to some extent even up to 1  $\mu\text{s}$  of simulation time for some systems. Given the derogatory effect of sub-diffusive dynamics on the accuracy of diffusivity predictions, we now explore how to better identify the extent of sub-diffusive dynamics for a given system for a given simulation duration. To do so, we consider scaling relationships useful in identifying diffusive and sub-diffusive regimes.

For the diffusive regime, displacements are Gaussian and satisfy the relation  $\langle \Delta r^2 \rangle \sim \Delta t^1$ . It is common in molecular dynamics studies of diffusion for the degree of diffusiveness to

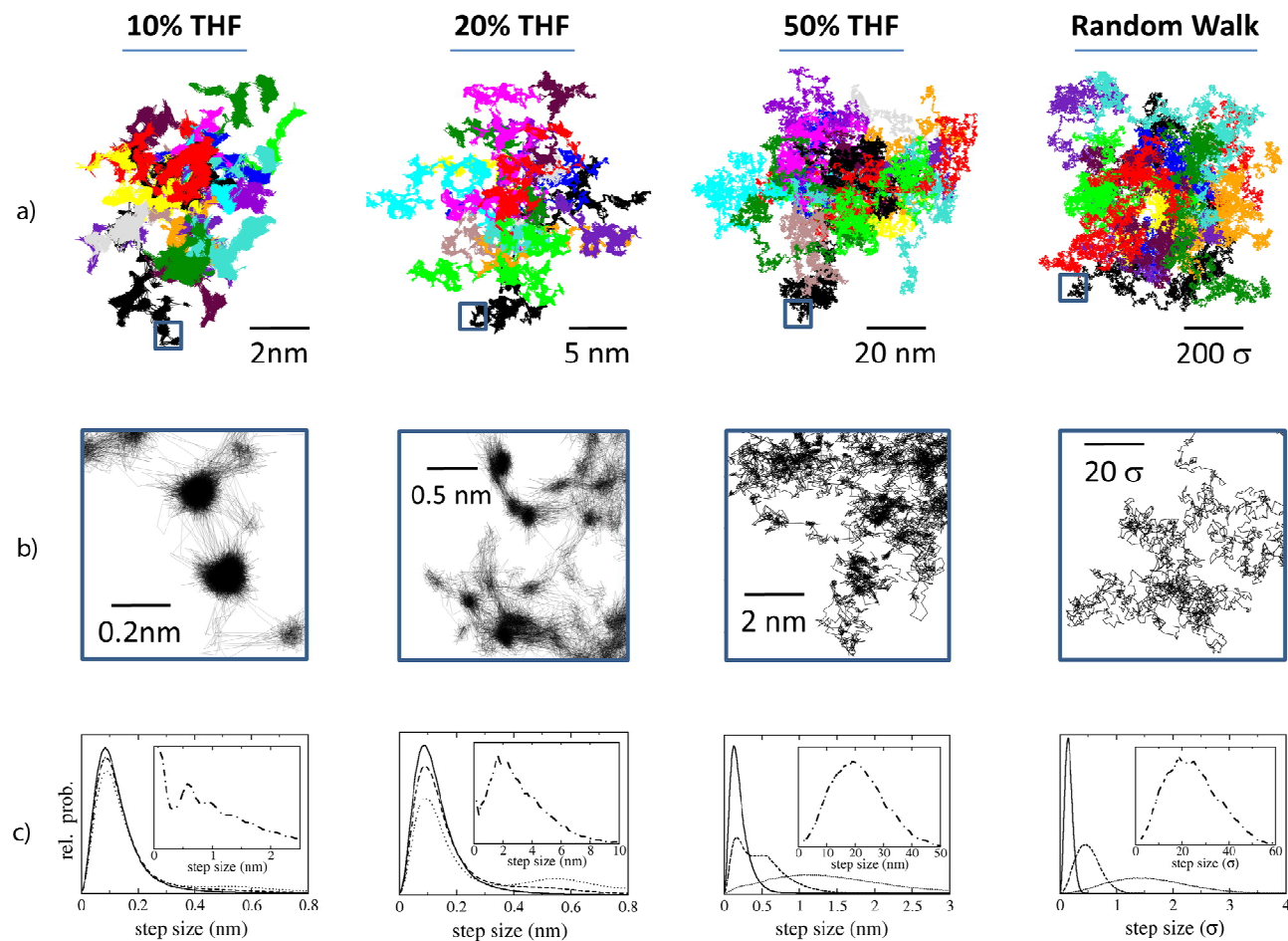


**Figure 5.** Individual molecular trajectories for THF/SIBS system. Each column represents a different THF concentration, indicated above. Random walk trajectories are provided at right for comparison. (a)  $1 \mu\text{s}$  trajectories of THF diffusion. Individual molecules are distinguished by color. (b) 10X magnification of  $\mu\text{s}$  trajectory from (a), with area of detail indicated by blue square. (c) Step size distribution as a function of time step: 10 ps (solid line), 100 ps (dashed line), 1 ns (dotted line), and 250 ns (dash-dot line).

be assessed based on the quality of the linear regression of  $\langle \Delta r^2 \rangle$  vs.  $\Delta t$ . However, it is difficult to distinguish by linear regression between the diffusive and the sub-diffusive regime, for which  $\langle \Delta r^2 \rangle \sim \Delta t^a$ , where the anomalous diffusion exponent,  $a$ , is somewhat less unity. The determination of the anomalous diffusion exponent,  $a$ , can be greatly improved by considering square displacement vs. time in log space, *i.e.*  $\log \langle \Delta r^2 \rangle$  vs.  $\log \Delta t$ , for which the slope is equal to  $a$ . In Figure 4b,  $\log \langle \Delta r^2 \rangle$  vs.  $\log \Delta t$  is plotted for each simulated system considered in this work. Regression in log space is a more rigorous test for convergence to the diffusive regime, as the slope must be both constant and equal to unity. A slope of unity is included (dashed line) for reference for each binary system in Figure 4b. The anomalous diffusion exponent,  $a$ , is seen to approach unity within a timeframe that is dependent upon the specific binary system and concentration. Determination of  $a$  not only provides a check on whether a given system has converged to the diffusive regime, it also provides useful

information on the time dependence of the approach to convergence. While a slope of unity is rapidly attained in systems with higher THF concentration, for glassier systems, particularly for the SIBS/TAC systems,  $a$  can be seen to approach, but not attain values of unity. These estimates of  $a$  corroborate the conclusion previously drawn from analysis of the time-dependence of step size distribution that sub-diffusive dynamics persists in proportion to the glassiness of a given system.

From Figure 4a and Figure 4b, it is evident that error in  $D_{\text{pred}}$  is most pronounced when  $a$  is far from unity; conversely, as  $a$  approaches unity, error in  $D_{\text{pred}}$  decreases dramatically. In principle, it should be possible to determine the relative error in  $D_{\text{pred}}$  as a function of  $a$ . Unfortunately, for our atomistic simulations, the mean squared displacement is too noisy to make sufficiently accurate determinations of  $a$  from the slope of  $\log \langle \Delta r^2 \rangle$  vs.  $\log \Delta t$  at any given time. For this reason, it is useful to consider an additional measure of the extent of sub-

diffusive dynamics, given by the ‘non-Gaussian parameter’,  $\alpha_2$ , *i.e.* the second cumulant of the ensemble average atomic displacement,<sup>90,91</sup>  $\alpha_2$  quantifies the extent to which displacements deviate from Gaussian behavior for a given  $\Delta t$ .  $\alpha_2$  is plotted as a function of  $\Delta t$  for each of our simulated systems in Figure 4c. The peak in  $\alpha_2$  provides useful information on the characteristic time at which dynamics begin to transition from the caged to the diffusive regime. As is true for  $D_{\text{pred}}$  and mean squared displacement, values of  $\alpha_2$  are subject to noise, likely a consequence of limitations on simulation duration and system size that come with atomistically detailed molecular dynamics simulations. Nonetheless, an approximate peak in  $\alpha_2$  can be discerned in Figure 4c for each simulated system. Comparing  $D_{\text{pred}}$  values in Figure 4a to  $\alpha_2$  values in Figure 4c for a given system,  $D_{\text{pred}}$  values appear to converge to within an order of magnitude of their final values prior to the  $\Delta t$  values corresponding to peaks in  $\alpha_2$ . This suggests that order of magnitude or better predictions of diffusivity can be obtained for simulations whose duration exceeds the  $\Delta t$  value corresponding to the peak in  $\alpha_2$ . It is thus encouraging to find that the  $\Delta t$  values corresponding to peak values of  $\alpha_2$  for TAC diffusion in TAC/SIBS systems are at least an order of magnitude less than the 1  $\mu\text{s}$  of simulation time in our work. Although we do not have experimental validation for this system, we have shown that accuracy of  $D_{\text{pred}}$  is dynamics-limited rather than force field limited. Thus, the fact that peaks in  $\alpha_2$  values for TAC/SIBS systems occur at timescales at least an order of magnitude less than our simulation duration strongly suggest that  $D_{\text{pred}}$  values should be within an order of magnitude of their true values.

We also note that, as  $D_{\text{pred}}$  decreases monotonically with simulation time,  $D_{\text{pred}}$  values for systems incompletely converged to the diffusive regime provide upper bounds on the true diffusivity. Knowledge of the upper bounds of diffusivity in polymer based systems would be particularly useful in the regulatory context as it would provide a means to determine the maximum patient exposure to a given leachable in a given period of time. This maximum potential exposure level could then in turn be compared to the established threshold of toxicological concern (TTC) level for a given leachable to make an informed assessment of the level of risk posed to the patient.

While useful information on diffusion can be obtained prior to complete convergence to the diffusive regime, sub-diffusive dynamics will continue to make diffusivity determinations slow and often prohibitively computationally intensive. Ever-increasing processing speeds will be helpful in overcoming error due to sub-diffusive dynamics, yet it will likely be years or decades before diffusivity can be calculated quickly and accurately for glassy systems and systems with larger diffusants. We conclude by introducing the possibility that more rapid simulation determinations of diffusivity may be possible with current limitations in processor speed by exploiting emerging relationships between fast and slow dynamics in systems with constrained dynamics, such as polymer/drug systems.

Work by Cicerone *et al.*<sup>94</sup> on the molecular basis of protein preservation in glassy molecular matrices at room temperature has demonstrated that protein stability, measured in months to years, correlates remarkably well with high frequency  $\beta$  relaxations of the matrix, which have a characteristic timescale on the order of femtoseconds. Cicerone *et al.* suggest that preservation time is a function of diffusion rate of small proteolytic molecules through the glassy matrix. This suggests a fundamental link between small molecule diffusion and the fast  $\beta$ -relaxation, which is itself closely related to the caging phenomenon detailed in our systems. Quantitative relationships<sup>95</sup> between fast and slow dynamics in glassy systems have recently been reported by Simmons *et al.*<sup>89, 96, 97</sup> and independently by Larini<sup>95</sup> and Puosi.<sup>98</sup> In particular, we use the generalized delocalization model of Simmons *et al.*,<sup>89</sup> which relates the segmental relaxation time,  $\tau$ , to the Debye-Waller factor  $\langle u^2 \rangle$ ,

$$\tau = \tau_0 \exp \left[ \left( \frac{u_0^2}{\langle u^2 \rangle} \right)^{\gamma/2} \right] \quad (7)$$

$\langle u^2 \rangle$  is equal to the square of the characteristic cage size of H-atoms of a system,  $\tau_0$  is a constant prefactor,  $u_0^2$  is the critical displacement required for cage escape, and  $\gamma$  is related to the temperature dependence of cage shape.  $\langle u^2 \rangle$  has been measured using neutron scattering<sup>99</sup> and can be determined from our simulation, as described below.  $\tau$  in turn has been suggested to be inversely proportional to diffusivity,<sup>10</sup> *i.e.*  $\tau \sim D^{-1}$ . We can thus relate long-time diffusion ( $D$ ) to fast dynamics ( $\langle u^2 \rangle$ ) using the expression

$$D = \frac{1}{\tau_0^*} \exp \left[ - \left( \frac{u_0^2}{\langle u^2 \rangle} \right)^{\gamma/2} \right] \quad (8)$$

where  $\tau_0^* = \tau_0 / c$  and  $c$  is a proportionality constant.

From our simulations, we determine  $\langle u^2 \rangle$  as the square of the displacement corresponding to the minimum of  $\delta(\log \langle \Delta r^2 \rangle) / \delta(\log \Delta t)$ , *i.e.* at the  $\Delta t$  corresponding to maximum caging. In Figure 6,  $D_{\text{pred}}$  vs.  $\langle u^2 \rangle$  is plotted for the THF/SIBS and THF/TAC systems. Values for fit parameters are as follows. For THF/SIBS,  $\tau_0^* = 639 \text{ s} / \text{cm}^2$ ,  $u_0 = 27 \text{ \AA}$ , and  $\gamma = 1.0$ . For THF/TAC,  $\tau_0^* = 0.1 \text{ s} / \text{cm}^2$ ,  $u_0 = 155 \text{ \AA}$ , and  $\gamma = 0.77$ . The fits are remarkably good, particularly given that the localization model of Simmons *et al.* was intended to apply to a given chemical system as a function of temperature, whereas, for our system, glassiness is adjusted by changing THF concentration at constant temperature. It is intriguing to note that the generalized localization model fits data over our entire concentration range, as it should be emphasized that the amount of simulation time required to converge  $D_{\text{pred}}$  values varies dramatically over this concentration range:  $D_{\text{pred}}$  values in the range of ( $10^{-6}$  to  $10^{-7}$ )  $\text{cm}^2 / \text{s}$  can be accurately simulated in a matter of hours to days, whereas slower diffusivity values can take months or longer to converge. The well-behaved relationship between  $D_{\text{pred}}$  and  $\langle u^2 \rangle$  reported herein suggests that more rapid assessment of diffusivity under glassier conditions relevant to drug and toxin leaching, currently

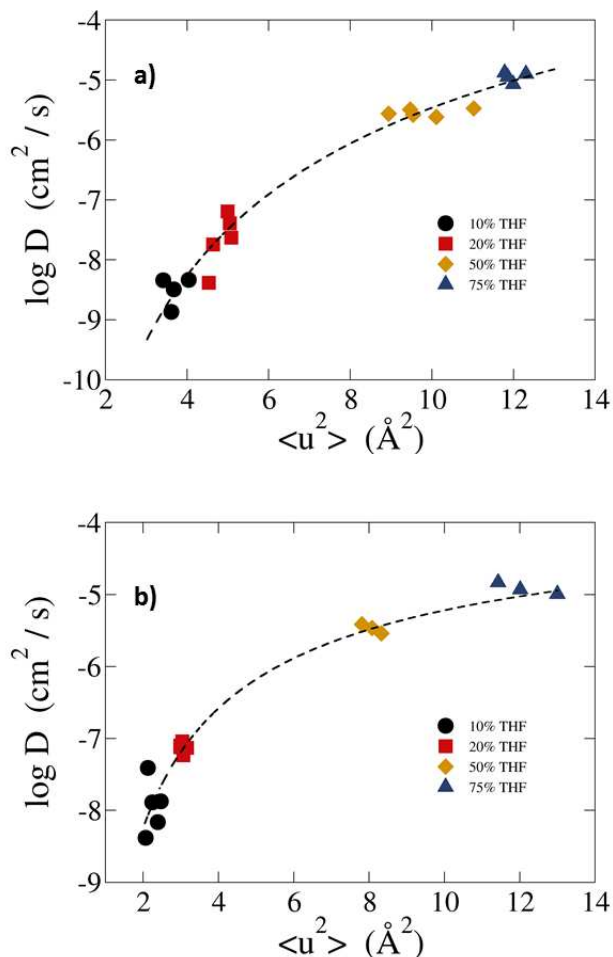


Figure 6. Predicted THF diffusivities vs.  $\langle u^2 \rangle$  for two systems: (a) THF/TAC; (b) THF/SIBS. THF concentrations are color coded consistently with Figure 4: 10% THF (black), 20% THF (red), 50% THF (gold), and 75% THF (blue). Individual symbols correspond to individual simulation runs for a given THF concentration. Dashed line is best fit to data using

(8).

requiring highly time-intensive simulations, may be achievable by probing dynamics in the less glassy regime, where short simulation durations are sufficient to accurately predict diffusivity. This approach requires that  $\langle u^2 \rangle$  can be rapidly determined over a wide range of system glassiness, including systems for which diffusivity predictions are time intensive. Fortunately, although  $D_{\text{pred}}$  predictions are most burdensome for glassy systems, the opposite is true for determinations of  $\langle u^2 \rangle$ , which can be rapidly determined in particular for more glassy systems, where caging arises most rapidly. We are currently developing this rapid assessment approach with promising initial results and will report our findings in a future manuscript.

## Conclusions

We have utilized atomistic molecular dynamics simulations to predict diffusivity in a model drug eluting stent coating, consisting of the drug tetracycline (TAC), the diblock copolymer poly(styrene-co-isobutylene-co-styrene) (SIBS), and the solvent tetrahydrofuran (THF). We have demonstrated that diffusivity can be accurately predicted given sufficient simulation duration, but that diffusivity is overestimated for simulations of insufficient duration. Such error is attributable to the presence of sub-diffusive or glassy dynamics, evidenced by non-Gaussian displacement and temporary localization, or ‘caging’, of the diffusing molecule. For glassier systems, we find that over-estimation of diffusivity decays monotonically with increasing simulation time. We have shown that sub-diffusive dynamics can persist to 1  $\mu\text{s}$  of simulation time for systems with highly constrained dynamics. Our results suggest that for systems similar to ours, *i.e.* systems in which small to medium sized molecules diffuse through a molecular matrix displaying time-dependent relaxational dynamics, the main obstacle to accurate diffusivity predictions is the lengthy simulation duration required to attain diffusive dynamics. On the other hand, accurate diffusivity predictions for our solvent rich (non-glassy) systems required less than 1 ns of simulation duration. Thus, our results suggest that diffusivity can be readily determined for solvent-rich systems, which are of broad relevance in controlled drug delivery applications, including swellable coatings and hydrogels.

We have performed vapor sorption analysis measurements of THF diffusion into drug/polymer coatings to validate a subset of our simulated systems. While vapor sorption measurements are limited to low THF concentration, it is precisely the low solvent regime for which glassy dynamics are prevalent and thus simulation predictions of diffusivity are most challenging. Our simulated predictions and vapor sorption measurements of diffusivity of THF in TAC and SIBS show remarkable agreement, particularly in comparison to previous published simulation predictions. We are unaware of previous simulation work that has accurately predicted diffusivity in comparable systems.

Finally, we have explored the possibility of more rapidly predicting diffusivity in slowly diffusing systems by employing a recent quantitative model relating fast and slow dynamics in constrained systems. In particular, we have shown that diffusivity is a function of the Debye-Waller factor, a quantity that can be readily determined by molecular dynamics simulation, thus presenting the possibility of making diffusivity determinations under rapidly converging conditions to predict diffusivity under slower converging conditions. In this work, we have outlined an approach for assuring accurate simulation predictions of diffusivity and established the foundation for making more computationally efficient diffusivity predictions in polymers and other systems with constrained dynamics.

## Acknowledgements

Simulations were made possible by access to high performance computational facilities through both the Division of Imaging

and Applied Mathematics (DIAM) and the Division of Electrical and Software Engineering (DESE) at the FDA. The authors acknowledge the financial support of the National Science Foundation (CBET-1041361) through the NSF/FDA Scholar-in-Residence Program at the FDA that provided support for E.M. Davis and Y.A. Elabd.

<sup>a</sup> Division of Chemistry and Materials Science, Center for Devices and Radiological Health, US Food and Drug Administration.

<sup>b</sup> Materials Science and Engineering Division, Materials Measurement Laboratory, National Institute of Standards and Technology.

<sup>c</sup> Department of Chemical and Biological Engineering, Drexel University, Philadelphia, Pennsylvania 19104.

<sup>1</sup>The mention of commercial products, their sources, or their use in connection with material reported herein is not to be construed as either an actual or implied endorsement of such products by the Department of Health and Human Services.<sup>22</sup>

†Certain commercial equipment, instruments, or materials are identified in this paper in order to specify the experimental procedure adequately. Such identification is not intended to imply recommendation or endorsement by the National Institute of Standards and Technology, nor is it intended to imply that the materials or equipment identified are necessarily the best available for the purpose.

## Notes and references

- R. Langer, *Accounts of Chemical Research*, 1993, **26**, 537-542.
- G. A. Buxton and N. Clarke, *Soft Matter*, 2007, **3**, 1513-1517.
- M. D. R. Rodriguez-Hidalgo, C. Soto-Figueroa and L. Vicente, *Soft Matter*, 2011, **7**, 8224-8230.
- F. Brandl, F. Kastner, R. M. Gschwind, T. Blunk, J. Tessmar and A. Gopferich, *Journal of Controlled Release*, 2010, **142**, 221-228.
- A. Beronius, C. Ruden, H. Hakansson and A. Hanberg, *Reproductive Toxicology*, 2010, **29**, 132-146.
- M. K. McDermott, D. M. Saylor, R. Casas, B. J. Dair, J. Guo, C. S. Kim, C. M. Mahoney, K. Ng, S. K. Pollack, D. V. Patwardhan, D. A. Sweigart, T. Thomas, J. Toy, C. M. Williams and C. N. Witkowski, *Journal of Pharmaceutical Sciences*, 2010, **99**, 2777-2785.
- C. Forrey, K. G. Yager and S. P. Broadaway, *Acs Nano*, 2011, **5**, 2895-2907.
- D. M. Saylor, C. S. Kim, D. V. Patwardhan and J. A. Warren, *Acta Biomaterialia*, 2007, **3**, 851-864.
- D. M. Saylor, C. S. Kim, D. V. Patwardhan and J. A. Warren, *Journal of Pharmaceutical Sciences*, 2009, **98**, 169-186.
- T. Cherdhirankorn, V. Harmandaris, A. Juhari, P. Voudouris, G. Fytas, K. Kremer and K. Koynov, *Macromolecules*, 2009, **42**, 4858-4866.
- T. A. Hunt and B. D. Todd, *Journal of Chemical Physics*, 2009, **131**.
- H. Sabbagh and B. C. Eu, *Physica a-Statistical Mechanics and Its Applications*, 2010, **389**, 2325-2338.
- P. Nazaran, V. Bosio, W. Jaeger, D. F. Anghel and R. von Klitzing, *Journal of Physical Chemistry B*, 2007, **111**, 8572-8581.
- A. Pluen, P. A. Netti, R. K. Jain and D. A. Berk, *Biophysical Journal*, 1999, **77**, 542-552.
- D. B. Hall, D. D. Deppe, K. E. Hamilton, A. Dhinojwala and J. M. Torkelson, *Journal of Non-Crystalline Solids*, 1998, **235**, 48-56.
- S. S. Jena and V. A. Bloomfield, *Macromolecules*, 2005, **38**, 10557-10560.
- D. D. Deppe, R. D. Miller and J. M. Torkelson, *Journal of Polymer Science Part B-Polymer Physics*, 1996, **34**, 2987-2997.
- M. Susoff and W. Oppermann, *Macromolecules*, 2010, **43**, 9100-9107.
- S. Matsukawa, H. Yasunaga, C. Zhao, S. Kuroki, H. Kurosu and I. Ando, *Progress in Polymer Science*, 1999, **24**, 995-1044.
- C. Ferrero, D. Massuelle, D. Jeannerat and E. Doelker, *Journal of Controlled Release*, 2008, **128**, 71-79.
- P. Occhipinti and P. C. Griffiths, *Advanced Drug Delivery Reviews*, 2008, **60**, 1570-1582.
- N. B. Hatzigrigoriou, C. D. Papaspyrides, C. Joly, J. Pinte and P. Dole, *Polymer Engineering and Science*, 2011, **51**, 532-541.
- J. Hansen and M. IR, *Theory of Simple Liquids*, New York: Academic, 1986.
- A. Einstein, *Annalen Der Physik*, 1905, **17**, 549-560.
- M. P. Allen and D. J. Tildesley, *Computer Simulation of Liquids*, Oxford University Press, 1989.
- R. J. Bearman and D. L. Jolly, *Molecular Physics*, 1981, **44**, 665-675.
- D. L. Jolly and R. J. Bearman, *Molecular Physics*, 1980, **41**, 137-147.
- M. Schoen and C. Hoheisel, *Molecular Physics*, 1984, **52**, 33-56.
- R. L. Rowley, S. C. Yi, V. Gubler and J. M. Stoker, *Fluid Phase Equilibria*, 1987, **36**, 219-233.
- J. M. Stoker and R. L. Rowley, *Journal of Chemical Physics*, 1989, **91**, 3670-3676.
- J. Liu, D. P. Cao and L. Q. Zhang, in *Journal of Physical Chemistry C*, Editon edn., 2008, vol. 112, pp. 6653-6661.
- P. B. Conrad and J. J. de Pablo, *Journal of Physical Chemistry A*, 1999, **103**, 4049-4055.
- Y. Y. Li and T. J. Hou, *Current Medicinal Chemistry*, 2010, **17**, 4482-4491.
- D. Bassolinoklimas, H. E. Alper and T. R. Stouch, *Journal of the American Chemical Society*, 1995, **117**, 4118-4129.
- C. J. Zhang and X. N. Yang, *Fluid Phase Equilibria*, 2005, **231**, 1-10.
- S. Bastea, *Soft Matter*, 2010, **6**, 4223-4228.
- H. T. Jung, B. J. Sung and A. Yethiraj, *Journal of Polymer Science Part B-Polymer Physics*, 2011, **49**, 818-825.
- Y. B. Wu, S. Joseph and N. R. Aluru, *Journal of Physical Chemistry B*, 2009, **113**, 3512-3520.
- J. Budzien, J. D. McCoy, D. Rottach and J. G. Curro, *Polymer*, 2004, **45**, 3923-3932.
- A. Gautieri, S. Vesentini and A. Redaelli, *Journal of Molecular Modeling*, 2010, **16**, 1845-1851.
- H. Masoud and A. Alexeev, *Macromolecules*, 2010, **43**, 10117-10122.
- J. Sonnenburg, J. Gao and J. H. Weiner, *Macromolecules*, 1990, **23**, 4653-4657.
- M. Meunier, *Journal of Chemical Physics*, 2005, **123**.
- S. Neyertz, D. Brown, S. Pandiyan and N. F. A. van der Vegt, *Macromolecules*, 2010, **43**, 7813-7827.
- E. Kucukpinar and P. Doruker, *Polymer*, 2003, **44**, 3607-3620.
- F. Mozaffari, H. Eslami and J. Moghadasi, *Polymer*, 2010, **51**, 300-307.
- D. Pavel and R. Shanks, *Polymer*, 2003, **44**, 6713-6724.
- S. Pricl and M. Ferneglia, *Chemical Engineering Communications*, 2003, **190**, 1267-1292.
- F. Mullerplathe, *Acta Polymerica*, 1994, **45**, 259-293.
- F. Mullerplathe, S. C. Rogers and W. F. Vangunsteren, *Macromolecules*, 1992, **25**, 6722-6724.
- S. G. Charati and S. A. Stern, *Macromolecules*, 1998, **31**, 5529-5535.
- J. Han and R. H. Boyd, *Macromolecules*, 1994, **27**, 5365-5370.
- G. E. Karlsson, U. W. Gedde and M. S. Hedenqvist, *Polymer*, 2004, **45**, 3893-3900.
- A. A. Gusev, S. Arizzi, U. W. Suter and D. J. Moll, *Journal of Chemical Physics*, 1993, **99**, 2221-2227.
- Y. Chen, Q. L. Liu, A. M. Zhu, Q. G. Zhang and J. Y. Wu, *Journal of Membrane Science*, 2010, **348**, 204-212.
- F. S. Pan, J. Ma, L. Cui and Z. Y. Jiang, *Chemical Engineering Science*, 2009, **64**, 5192-5197.
- M. M. Ostwal, T. T. Tsotsis and M. Sahimi, *Journal of Chemical Physics*, 2007, **126**.

58. V. A. Harmandaris, N. P. Adhikari, N. F. A. van der Vegt, K. Kremer, B. A. Mann, R. Voelkel, H. Weiss and C. C. Liew, *Macromolecules*, 2007, **40**, 7026-7035.
59. Q. G. Zhang, Q. L. Liu, Y. Chen, J. Y. Wu and A. M. Zhu, *Chemical Engineering Science*, 2009, **64**, 334-340.
60. Z. X. Chen, Q. Gu, H. F. Zou, T. Q. Zhao and H. Y. Wang, *Journal of Polymer Science Part B-Polymer Physics*, 2007, **45**, 884-891.
61. F. S. Pan, F. B. Peng and Z. Y. Jiang, *Chemical Engineering Science*, 2007, **62**, 703-710.
62. C. D. Yoo, S. C. Kim and S. H. Lee, *Molecular Simulation*, 2009, **35**, 241-247.
63. M. Tsige and G. S. Grest, *Journal of Chemical Physics*, 2004, **120**, 2989-2995.
64. M. Fukuda and S. Kuwajima, *Journal of Chemical Physics*, 1998, **108**, 3001-3009.
65. Z. J. Zhao, Q. Wang, L. Zhang and Y. C. Liu, *Journal of Physical Chemistry B*, 2007, **111**, 4411-4416.
66. F. Faure, B. Rousseau, V. Lachet and P. Ungerer, *Fluid Phase Equilibria*, 2007, **261**, 168-175.
67. R. K. Bharadwaj and R. H. Boyd, *Polymer*, 1999, **40**, 4229-4236.
68. J. Han and R. H. Boyd, *Polymer*, 1996, **37**, 1797-1804.
69. O. Hahn, D. A. Mooney, F. Muller-Plathe and K. Kremer, *Journal of Chemical Physics*, 1999, **111**, 6061-6068.
70. V. A. Harmandaris and K. Kremer, *Macromolecules*, 2009, **42**, 791-802.
71. T. L. Li, D. O. Kildsig and K. Park, *Journal of Controlled Release*, 1997, **48**, 57-66.
72. C. S. Kim, D. M. Saylor, M. K. McDermott, D. V. Patwardhan and J. A. Warren, *Journal of Biomedical Materials Research Part B-Applied Biomaterials*, 2009, **90B**, 688-699.
73. D. N. Theodorou and U. W. Suter, *Macromolecules*, 1985, **18**, 1467-1478.
74. S. Plimpton, *Journal of Computational Physics*, 1995, **117**, 1-19.
75. J. M. Wang, R. M. Wolf, J. W. Caldwell, P. A. Kollman and D. A. Case, *Journal of Computational Chemistry*, 2004, **25**, 1157-1174.
76. M. G. Baschetti, E. Piccinini, T. A. Barbari and G. C. Sarti, *Macromolecules*, 2003, **36**, 9574-9584.
77. J. L. Duda, Y. C. Ni and J. S. Vrentas, *Macromolecules*, 1979, **12**, 459-462.
78. S. Torquato, *Random Heterogeneous Materials: Microstructure and Macroscopic Properties*, Springer, 2006.
79. J. S. Vrentas and J. L. Duda, *Journal of Polymer Science Part B-Polymer Physics*, 1977, **15**, 403-416.
80. M. T. Cicerone, F. R. Blackburn and M. D. Ediger, *Macromolecules*, 1995, **28**, 8224-8232.
81. R. E. Hoffman, E. Shabtai, M. Rabinovitz, V. S. Iyer, K. Mullen, A. K. Rai, E. Bayrd and L. T. Scott, *Journal of the Chemical Society-Perkin Transactions 2*, 1998, 1659-1664.
82. S. U. Hong, T. A. Barbari and J. M. Sloan, *Journal of Polymer Science Part B-Polymer Physics*, 1997, **35**, 1261-1267.
83. C. Forrey, J. F. Douglas and M. K. Gilson, *Soft Matter*, 2012, **8**, 6385-6392.
84. C. Forrey and M. Muthukumar, *Biophysical Journal*, 2006, **91**, 25-41.
85. R. H. Gee and R. H. Boyd, *Polymer*, 1995, **36**, 1435-1440.
86. A. A. Gusev, F. Mullerplathe, W. F. Vangunsteren and U. W. Suter, *Atomistic Modeling of Physical Properties*, 1994, **116**, 207-247.
87. A. A. Gusev and U. W. Suter, *Journal of Chemical Physics*, 1993, **99**, 2228-2234.
88. H. F. M. Mohamed, Y. Kobayashi, C. S. Kuroda and A. Ohira, *Journal of Physical Chemistry B*, 2009, **113**, 2247-2252.
89. D. S. Simmons, M. T. Cicerone, Q. Zhong, M. Tyagi and J. F. Douglas, *Soft Matter*, 2012, **8**, 11455-11461.
90. M. S. Shell, P. G. Debenedetti and F. H. Stillinger, *Journal of Physics-Condensed Matter*, 2005, **17**, S4035-S4046.
91. D. Bedrov, G. Smith and J. F. Douglas, *Polymer*, 2004, **45**, 3961-3966.
92. M. D. Ediger, *Annual Review of Physical Chemistry*, 2000, **51**, 99-128.
93. B. M. I. Flier, M. C. Baier, J. Huber, K. Mullen, S. Mecking, A. Zumbusch and D. Woll, *Journal of the American Chemical Society*, 2012, **134**, 480-488.
94. M. T. Cicerone and J. F. Douglas, *Soft Matter*, 2012, **8**, 2983-2991.
95. L. Larini, A. Ottochian, C. De Michele and D. Leporini, *Nature Physics*, 2008, **4**, 42-45.
96. D. S. Simmons, M. T. Cicerone and J. F. Douglas, *Biophysical Journal*, 2011, **100**, 228-228.
97. D. S. Simmons and J. F. Douglas, *Soft Matter*, 2011, **7**, 11010-11020.
98. F. Puosi and D. Leporini, *Journal of Physical Chemistry B*, 2011, **115**, 14046-14051.
99. M. T. Cicerone and C. L. Soles, *Biophysical Journal*, 2004, **86**, 3836-3845.

